International Journal of Heat and Technology
Vol. 44, No. 2, April, 2026, pp. 602-612
Journal homepage: http://iieta.org/journals/ijht

Optimizing Heat Transfer and Pressure Drop in Shell-and-Tube Heat Exchangers: A Comparative Study of Segmental and Helical Baffles

James Julian[1], Fitri Wahyuni[1], Muhammad Ilham Adhynugraha[2], Fadilah Hasim[2], Adi Winarta[3*], I Nyoman Agus Adi Saputra[3]

[1] Department of Mechanical Engineering, Universitas Pembangunan Nasional Veteran Jakarta, Jakarta 12450, Indonesia
[2] National Research and Innovation Agency (BRIN), Jakarta 10340, Indonesia
[3] Department of Mechanical Engineering, Politeknik Negeri Bali, Kampus Bukit Jimbaran Bali, Jimbaran 80364, Indonesia

Corresponding Author Email: adi.winarta@pnb.ac.id

https://doi.org/10.18280/ijht.440214

Received: 27 November 2025
Revised: 9 February 2026
Accepted: 18 February 2026
Available online: 30 April 2026

Keywords:
segmental baffles - shell-and-tube heat exchangers, helical baffles, performance evaluation factor, computational fluid dynamics simulations, baffle pitch optimization

ABSTRACT

This study investigates the performance of different baffle configurations in shell-and-tube heat exchangers (STHE), specifically comparing segmental baffles (SB) with helical baffles (HB) at varying pitch distances (40 mm, 50 mm, and 60 mm). Using computational fluid dynamics (CFD) simulations with ANSYS Fluent, the effects of baffle design on heat transfer efficiency and pressure drop were analysed across different mass flow rates. The results show that while the 40 mm pitch HB configuration exhibited the highest heat transfer coefficient ($\propto$), it also led to the highest pressure drop. In contrast, the 60 mm pitch HB configuration achieved the lowest pressure drop and a balanced heat transfer performance, making it the most optimal design. Performance evaluation factor (PEF) analysis confirmed that the 60 mm HB configuration offered the best overall efficiency, striking an ideal balance between thermal performance and reduced pumping power. This study underscores the importance of optimizing baffle pitch in STHE to maximize energy efficiency and reduce operational costs. The findings suggest that helical baffles, particularly with a 60 mm pitch, provide the most favourable design for industrial applications where both high heat transfer and low-pressure loss are required. The study offers valuable insights into optimising heat exchanger design, contributing to more energy-efficient and cost-effective thermal systems.

1. INTRODUCTION

Shell-and-tube heat exchangers (STHE) are widely used in various industries due to their simple design, high versatility, and effectiveness in heat transfer. These exchangers operate on the principle of heat transfer between two fluids at different temperatures, transferring thermal energy from the hotter to the cooler fluid, resulting in cooling of the hotter fluid and heating of the cooler one [1]. The flexibility of STHE allows use in chemical engineering, power generation, petroleum refining, refrigeration, and the food industry [2]. Compared to other heat exchangers, shell-and-tube designs are simpler to manufacture, cost-effective, and adaptable to various operational needs [3, 4]. Over 30% of heat exchangers in operation today are shell-and-tube types, highlighting their continued importance [5, 6].

Critical component in STHE design and performance is the baffle, which regulates fluid flow, enhances heat transfer, and prevents tube vibrations. Baffles support the tube bundle, direct shell-side fluid flow, and create turbulence, increasing the heat transfer coefficient by improving contact between hot and cold fluids [7]. Traditionally, single segmental baffles (SB) are commonly used, forcing fluid to flow in a zigzag pattern, promoting turbulence, local mixing, and improving heat transfer. However, SB have inherent limitations affecting efficiency and operational costs [8].

The performance of STHE is significantly influenced by baffle design, with helical baffles (HB) offering advantages over SB. HB eliminates dead zones, reduces pressure drops, and minimizes tube bundle vibrations, improving heat transfer efficiency [9]. Studies by Kral et al. [10] and Gao et al. [11] showed that adjusting the HB angle optimizes heat transfer while controlling pressure drop, with the latter using the second law of thermodynamics to assess flow resistance. Studies by Almulla et al. [12] also indicate that optimized baffle configurations lead to substantial operational improvements. Comparative analyses by Sun et al. [13] consistently show HB outperforming SB and other baffle configurations in heat transfer efficiency and pressure drop characteristics. Numerical investigations by Yang et al. [14] and Li and Kottke [7] confirm the superior performance of HB. Additionally, Pal et al. [15] found that complex flow patterns significantly impact STHE efficiency. Other studies, such as those by Xiao et al. [16], contributed to understanding the role of crossover temperature and the effect of the Prandtl number on heat transfer. These studies highlight the crucial role of baffle configuration in optimizing STHE's thermal and hydraulic performance, demonstrating efficiency gains

achievable through properly configured HB.

In response to these challenges, the heat exchanger industry has increasingly adopted alternative baffle designs, such as HB, to improve both heat transfer and operational efficiency. HB facilitates a more uniform fluid flow, reducing issues with stagnant zones and flow separation [17]. Flow simulations of STHE with HB show continuous helical flow, enhancing fluid mixing and improving the heat transfer coefficient while reducing the pressure drop compared to SB [17]. Reducing stagnant zones also leads to lower fouling rates and minimizes potential erosion and corrosion within the shell, improving the heat exchanger's lifespan and overall performance.

The design of HB, particularly pitch, plays a crucial role in determining STHE's thermo-hydraulic performance. Several studies have shown that adjusting HB pitch can optimize heat transfer while minimizing pressure drop. Zhang et al. [9] found that varying pitch influences heat transfer and pressure drop, with smaller pitches increasing turbulence and heat transfer at the cost of higher pressure drops. Larger pitches reduce turbulence and pressure drop but may reduce thermal performance. These findings align with Zhang et al. [18], who showed pitch variation directly impacts flow behavior and thermal-hydraulic outcomes. Given these trade-offs, optimizing HB pitch is essential to balance heat transfer efficiency and operational performance, minimizing energy consumption and operational costs.

Growing interest in alternative baffle designs, such as helical and trefoil-hole baffles, arises from the need to optimize STHE performance in terms of heat transfer and operational costs. This is particularly important in industries where energy consumption and operational costs are significant. In SB heat exchangers, high pressure drops increase pumping power, elevating operational costs and reducing system efficiency [14]. Tanujaya et al. [19] and Naqvi et al [20] noted that SB restricts flow and increases hydraulic losses. In contrast, helical and trefoil-hole baffles significantly reduce pressure drops, enhance fluid mixing, and improve heat transfer, making them a more energy-efficient choice for industrial heat exchangers [4, 13]. Additionally, variations in HB pitch improve STHE operational sustainability and thermo-hydraulic performance [21].

Despite extensive studies on STHE with HB, several limitations remain. Most studies focus on global performance indicators like average heat transfer coefficient or pressure drop, without fully analyzing the flow mechanisms behind the trade-off between thermal enhancement and hydraulic penalty. Many comparative studies assess different baffle configurations under varying geometric or operational conditions, complicating the identification of optimal designs from an energy-efficiency perspective. Systematic evaluations directly linking HB pitch variation to flow structure evolution, thermo-hydraulic performance, and performance evaluation factor (PEF) under identical operating conditions are still limited.

To address these gaps, the present study provides a controlled comparative numerical investigation of segmental and HB configurations using identical geometric and operating parameters. The study systematically evaluates the influence of HB pitch (40, 50, and 60 mm) on flow characteristics, pressure drop, heat transfer coefficient, and overall thermo-hydraulic efficiency using the PEF. By linking flow structure behavior to observed thermo-hydraulic performance, this work offers a clearer mechanistic interpretation of the trade-off between heat transfer enhancement and hydraulic resistance, providing practical guidance for energy-efficient baffle design in industrial STHE.

2. METHODS

2.1 Numerical setup

This study numerically investigates the thermal–hydraulic performance of STHE equipped with segmental and HB. A double-tube plate shell-and-tube heat exchangers (DTP-STHE) configuration is adopted, with its geometry shown in Figure 1 and key parameters summarized in Table 1. To ensure a fair comparison, all geometric and operating parameters are kept identical for all cases, except for the baffle configuration, following the methodology of He and Li [22]. Water is used as the working fluid on both the shell and tube sides. Due to the relatively small temperature variations, the thermophysical properties of water and carbon steel are assumed constant, as listed in Table 2. All solid components of the STHE are made of carbon steel.

The effect of HB pitch on heat transfer enhancement is examined by varying the pitch distance to 40 mm, 50 mm, and 60 mm, while the SB configuration is used as a reference. The corresponding baffle arrangements are illustrated in Figures 2–4.

Table 1. Geometry parameters of the segmental and helical baffle (HB)

Item	Dimensions		Unit
Baffle Shape	Segmental 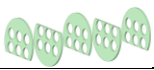	Helical 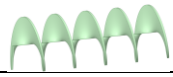	
D_s	87	87	mm
L_H	500	500	mm
d_O	19	19	mm
T_t	1.5	1.5	mm
L	365	365	mm
P_t	24	24	mm
N_T	6	6	–
B_s	57	57	mm
B_t	3	3	mm
$S_{i/o}$	61	61	mm
D_n	35.8	35.8	mm
B_c	25	–	%

Table 2. Thermo-physical properties of shell-and-tube heat exchangers (STHE)

Parameter	Value			Unit
	Hot Water	Cold Water	Carbon Steel	
λ	0.66	0.60	45	$W \cdot m^{-1} \cdot K^{-1}$
μ	0.00037	0.001	–	$kg \cdot m^{-1} \cdot s^{-1}$
ρ	974	998	7840	$kg \cdot m^{-3}$
C_p	4194	4182	490	$J \cdot kg^{-1} \cdot K^{-1}$

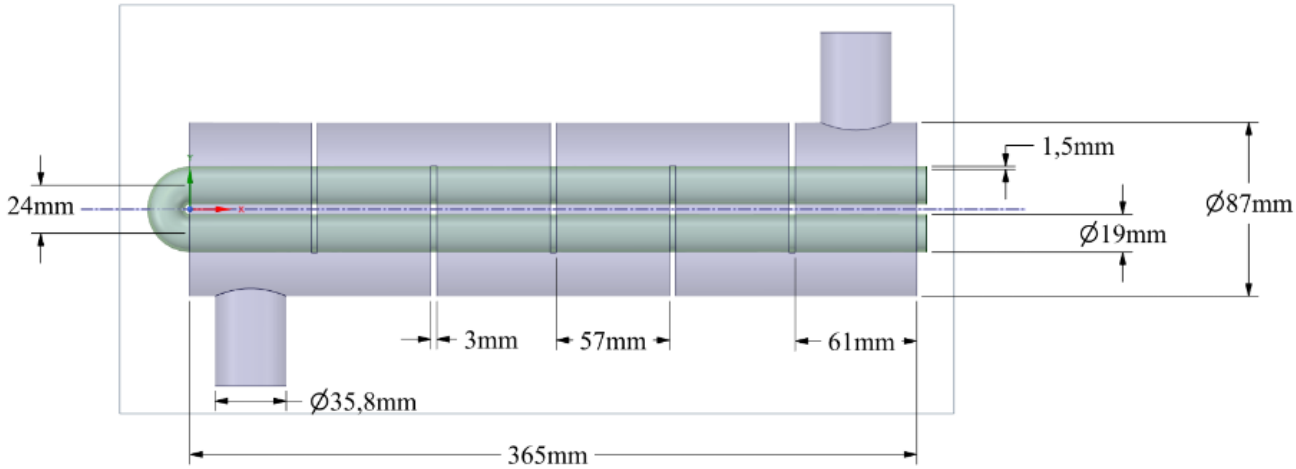

Figure 1. Geometry of segmental baffles - shell-and-tube heat exchangers (SB-STHE)

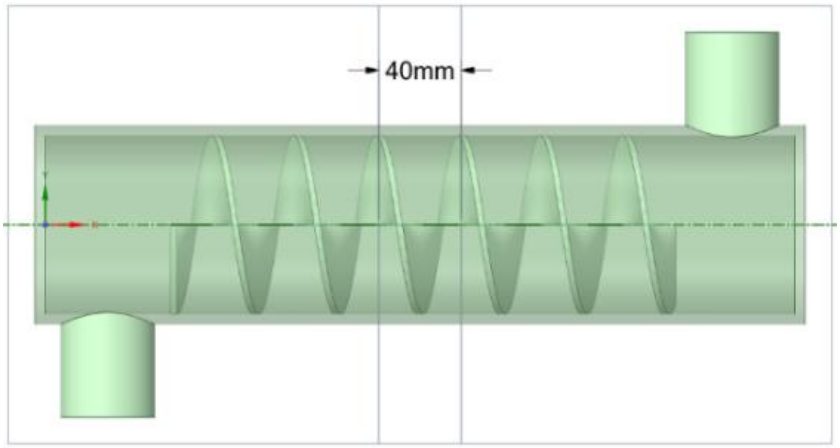

Figure 2. Helical baffle (HB) with baffle pitch 40 mm

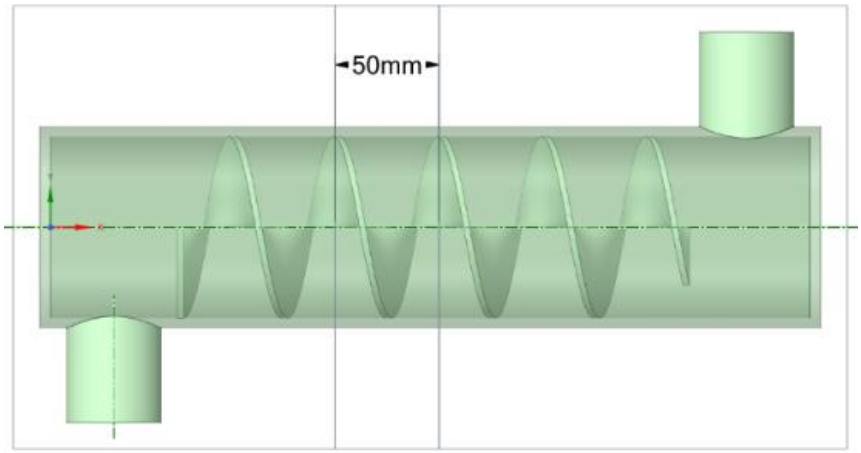

Figure 3. Helical baffle (HB) with baffle pitch 50 mm

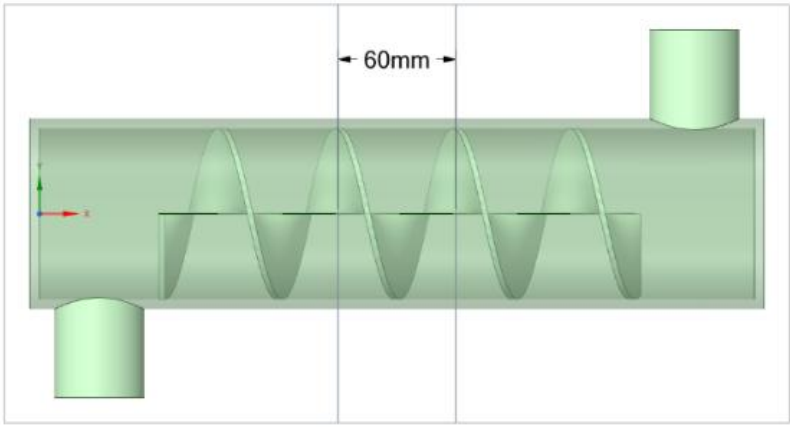

Figure 4. Helical baffle (HB) with baffle pitch 60 mm

Table 3. Set up parameters on shell-and-tube heat exchangers (STHE)

Item	Value		Unit
Location	Shell	Tube	
Mass flow inlet	1.1, 1.3, 1.5, 1.7, 1.9	0.2	kg/s
Pressure outlet	0	0	Pa
Temperature	353.15	293.15	K
Hydraulic diameter	87	16	mm
Gravity	–9.81 ($Y - axis$)		m/s^2

Table 4. Solution parameters on shell-and-tube heat exchangers (STHE)

Parameter	Item
Governing equation	Finite-volume method
Scheme	SIMPLE
Gradient	Least squares cell based
Pressure	Standard
Momentum Turbulent kinetic energy Turbulent dissipation rate Energy	Second order upwind

Table 5. Variation of different element systems

System	Total nodes	Total elements	Avg. element Quality	Avg. Skewness	Avg. Orthogonal Quality
System 1	387134	1847173	0.84429	0.21314	0.78562
System 2	501018	2430184	0.84611	0.21178	0.78697
System 3	667691	3297399	0.84709	0.21119	0.78761

Table 6. Mesh quality for each baffle pitch variation

Baffle Type	Total Nodes	Total Elements	Avg. Element Quality	Avg. Skewness	Avg. Orthogonal Quality
Segmental	501018	2430184	0.84611	0.21178	0.78697
Helical ($P_b = 60$ mm)	504773	2443993	0.84466	0.21383	0.78502
Helical ($P_b = 50$ mm)	504110	2433624	0.84474	0.21378	0.78505
Helical ($P_b = 40$ mm)	502525	2417819	0.84475	0.21369	0.78513

Computational fluid dynamics (CFD) simulations are performed using ANSYS Fluent in a three-dimensional, steady-state framework. Turbulence is modeled using the RNG k–ε model, which is suitable for swirling and secondary flows commonly induced by HB. The governing equations include the continuity, momentum, energy, turbulent kinetic energy (k), and turbulent dissipation rate (ε) equations, with standard RNG model constants applied.

Mass-flow inlet boundary conditions are imposed at both shell- and tube-side inlets, while pressure-outlet conditions are specified at the outlets. All walls are treated as no-slip boundaries. Zero heat flux is applied to the shell and nozzle walls, while conjugate heat transfer is considered between the tube wall and shell-side fluid. Standard wall functions are employed, with a target y+ value of approximately 300 to reduce computational cost.

The mathematical model used in this study is based on the following governing equations:

Continuity equation:

$$\frac{\partial(\rho u_i)}{\partial x_i} = 0 \tag{1}$$

Momentum transport equation:

$$\frac{\partial(\rho u_i u_k)}{\partial x_i} = -\frac{\partial_P}{\partial x_k} + \frac{\partial}{\partial x_i}\left(u_{eff}\ \frac{\partial u_k}{\partial x_i}\right) \quad (2)$$

Energy equation:

$$\frac{\partial(\rho u_i T)}{\partial x_i} = \frac{\partial}{\partial x_i}\left[\left(\frac{\mu}{Pr} + \frac{\mu_t}{\sigma_T}\right)\frac{\partial T}{\partial x_i}\right] \quad (3)$$

Turbulent kinetic energy:

$$\frac{\partial(\rho k u_i)}{\partial x_i} = \frac{\partial}{\partial x_i}\left[a_k \mu_{eff}\ \frac{\partial k}{\partial x_j}\right] + G_k + \rho_\varepsilon \quad (4)$$

Turbulent dissipation energy:

$$\frac{\partial(\rho \varepsilon u_i)}{\partial x_i} = \frac{\partial}{\partial x_i}\left[a_\varepsilon \mu_{eff}\ \frac{\partial \varepsilon}{\partial x_j}\right] + C_{1\varepsilon}^{*}\frac{\varepsilon}{k}\ G_{k-}\ C_{2\varepsilon}\rho\frac{\varepsilon^2}{k} \quad (5)$$

where,

$$\begin{cases} u_{eff} = \mu + \mu_t \\ \mu_t = \rho C_\mu \dfrac{k^2}{\varepsilon} \\ C_\mu = 0.0845, \alpha_k = \alpha_\varepsilon = 1.39 \\ C_{1\varepsilon}^{*} = C_{1\varepsilon} - \dfrac{\eta\left(1-\frac{\eta}{\eta_0}\right)}{1+\beta\eta^3} \\ C_{1\varepsilon} = 1.42, C_{2\varepsilon} = 1.68 \\ \eta = \left(2E_{ij}E_{ji}\right)\dfrac{1}{2}\dfrac{k}{\varepsilon} \\ E_{ij} = \dfrac{1}{2}\left(\dfrac{\partial_{ui}}{\partial x_j} + \dfrac{\partial_{uj}}{\partial x_i}\right) \\ \eta_0 = 4.377, \beta = 0.012 \\ \sigma_{T=(0.9\ \sim 1.0)} \end{cases} \quad (6)$$

The boundary conditions for the STHE are in Table 3, and the solution parameters for CFD simulations are in Table 4. Table 5 shows the mesh element variations from the mesh independence study. Unstructured meshes are generated with local refinement near tube–baffle interactions. A mesh independence study with three mesh densities shows pressure drop and heat transfer coefficient variations of less than 1% between the two finest meshes. Thus, the mesh system 2 with 2,430,184 elements is selected. Mesh quality metrics meet ANSYS Fluent criteria (Table 6). Convergence is achieved with default residuals, except for the energy equation set to 10^{-7}. Key variables, such as temperature, pressure, and mass flow rate, are monitored for stability and accuracy.

2.2 Data reduction

2.2.1 Heat rate and shell-side heat transfer coefficient

$\dot{Q}_c$ is the heat transferred to the cold fluid, which can be calculated by the following equation:

$$\dot{Q}_c = G_c\ x\ C_{p,c}\ x\ (t_{out,c} - t_{in,c}) \quad (7)$$

$\dot{Q}_h$ is the heat released by hot water, which can also be calculated in the following way:

$$\dot{Q}_h = G_h\ x\ C_{p,h}\ x\ (t_{in,h} - t_{out,h}) \quad (8)$$

The heat transfer between the STHE and the environment is neglected, so the heat transfer rate on the cold side ($\dot{Q}_c$) is assumed to be equal to the heat transfer rate on the hot side ($\dot{Q}_h$). The shell-side heat transfer coefficient ($\propto_s$) is a critical parameter in this study and is defined by the following equation:

$$\propto_s = \frac{\dot{Q}_h}{A_0.\Delta t_m} \quad (9)$$

Δt_m can be calculated by:

$$\begin{cases} A_0 = n.\pi.d_o, l \\ \Delta t_m = \dfrac{\Delta t_{max} - \Delta t_{min}}{\ln\left(\frac{\Delta t_{max}}{\Delta t_{min}}\right)} \\ \Delta t_{max} = max\left(t_{h,in} - t_{c.out}\ , t_{h,in} - t_{c.out}\right) \\ \Delta t_{min} = min\left(t_{h,in} - t_{c.out}\ , t_{h,in} - t_{c.out}\right) \end{cases} \quad (10)$$

2.2.2 Pressure drops

In this case, if the potential energy is neglected, the total pressure drop can be expressed as follows:

$$\Delta P_t = \Delta P_s + \Delta P_d \quad (11)$$

2.2.3 Determination of shell side V_s and Re_s number

For the mean shell side velocity (V_s) is defined using the equation:

$$V_s = \frac{G_h}{\rho_s.A_{cross}} \quad (12)$$

A_{cross} for the SB are as follows:

$$A_{cross} = (D_s - N_C.d_o).B \quad (13)$$

A_{cross} for HB:

$$A_{cross} = 0.5(D_s - N_C.d_o).B \quad (14)$$

Reynolds number on the shell side (Re_s) can be calculated by:

$$Re_s = \frac{V_s.\ d_e.\rho_s}{\mu_s} \quad (15)$$

For the layout of the square tube, d_e can be obtained from the equation below:

$$d_e = \frac{D_S^2 - N_T.d_o^2}{D_s + N_T.d_o} \quad (16)$$

2.3 Model validation

The model validation in this study was performed by comparing the numerical results with experimental data previously obtained by He and Li [22]. The comparison parameters included pressure drop (ΔP) and heat transfer coefficient ($\propto_s$) at different Reynolds numbers. Figures 5 and 6 show this comparison between our proposed model and the experimental results from He and Li [22]. As illustrated in the graphs, the average differences between our model and their

results are 2.9% for ΔP and 5.74% for $\propto_s$ in terms of pressure drop, and 0.82% and 4.95% for the heat transfer coefficient, respectively [22].

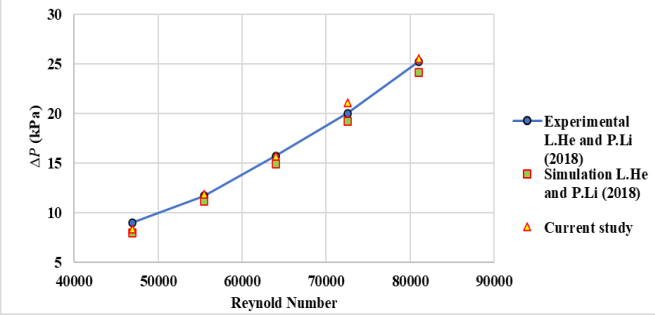

Figure 5. Comparison of the pressure drops between experimental and simulation results

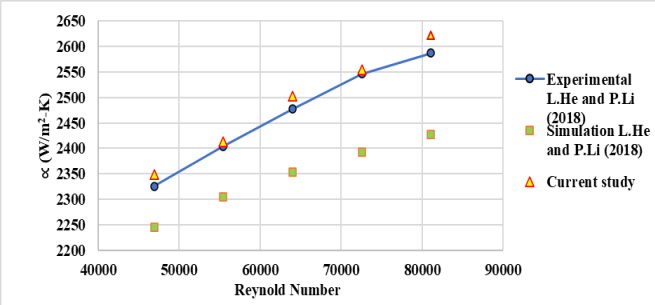

Figure 6. Comparison of the heat transfer coefficient between experimental and simulation results

3. RESULT AND DISCUSSION

This section presents the results obtained from the numerical simulations performed on four different baffle configurations for STHE: SB and HB with pitch distances of 40 mm, 50 mm, and 60 mm. The results are discussed regarding the flow field characteristics, pressure drop, heat transfer coefficient, and PEF across different mass flow rates.

3.1 Flow field characteristics on the shell side

The flow field characteristics for each baffle configuration were analysed using CFD simulations. Figure 7–10 presents the velocity streamlines and flow patterns for the four configurations: SB and HB with 40 mm, 50 mm, and 60 mm pitch distances.

For the SB configuration (Figure 7), the axial flow is forced to change direction due to the baffle cut, creating a zigzag flow pattern. This zigzag flow is intended to induce turbulence, enhancing heat transfer, as widely reported in the literature [18]. However, the abrupt changes in flow direction also lead to significant recirculation and the formation of stagnation zones near the back of the baffle plates, consistent with findings by Vukić Mića et al. [23] and Pamuk [24]. These stagnation zones reduce fluid velocity and contribute to higher pressure drops within the shell. The fluid velocity decreases significantly as it moves against gravity, leading to a situation where the fluid can become nearly stagnant, especially at lower mass flow rates. This pattern contributes to the high pressure drop observed in systems with SB, as the fluid flow is interrupted and disturbed by the geometry of the baffles. Although this configuration increases the turbulence intensity and heat transfer coefficient ($\propto_s$), the resultant pressure drop (ΔP) is considerably high.

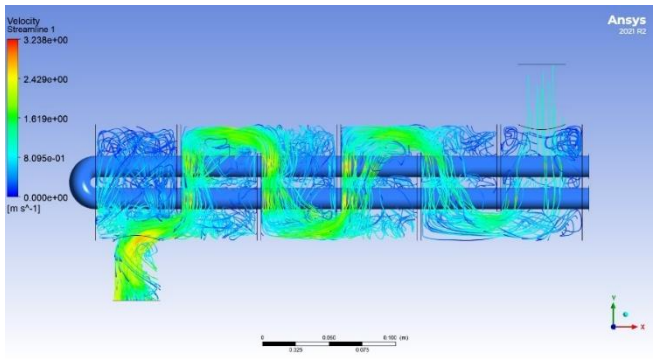

Figure 7. Flow field characteristics of the segmental baffle (SB)

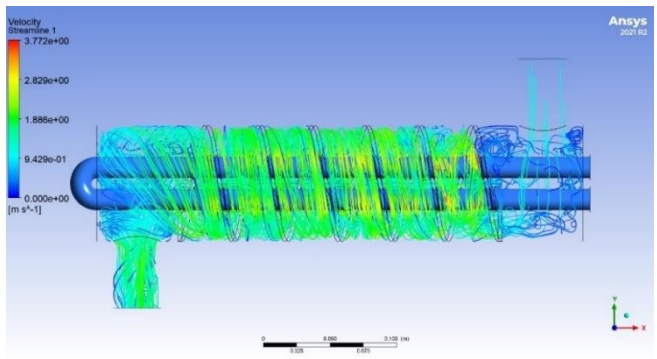

Figure 8. Flow field characteristics of helical baffle (HB) with baffle pitch 40 mm

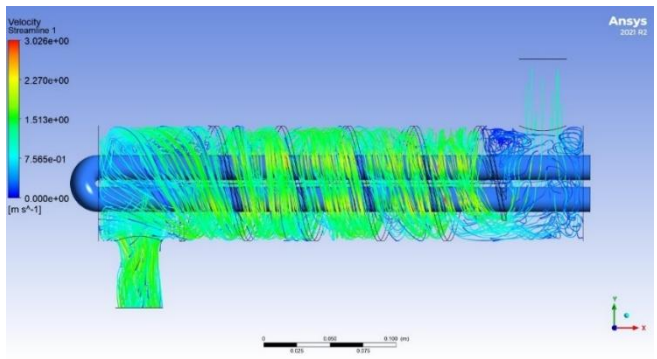

Figure 9. Flow field characteristics of helical baffle (HB) with baffle pitch 50 mm

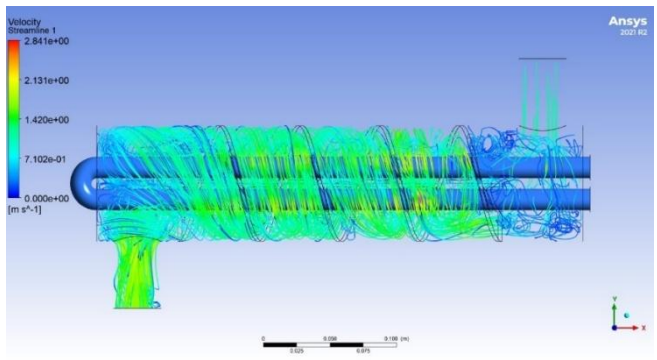

Figure 10. Flow field characteristics of helical baffle (HB) with baffle pitch 60 mm

In contrast, the HB configurations (Figures 8–10) generate a more uniform and continuous flow pattern due to the spiral motion imposed on the shell-side fluid. This spiral flow enhances fluid velocity distribution and significantly reduces the formation of stagnation zones, as demonstrated by Wen et al. [25] and De et al. [26]. The improved circulation allows the fluid to move more evenly around the tube bundle, resulting in better mixing and enhanced heat transfer performance, consistent with observations by Song [27]. The effect of pitch variation is also evident: at smaller pitch distances (40 mm), higher local fluid velocities intensify turbulence and mixing, aligning with findings from Rahmah et al. [28]. As the pitch increases to 50 mm and 60 mm, the flow becomes more uniform with reduced turbulence intensity, leading to lower pressure drops across the shell side, as reported by Yousfi [29]. Overall, HB configurations, particularly at a 60 mm pitch, promote more stable flow behavior and achieve efficient heat transfer with reduced flow resistance compared to the SB configuration.

3.2 Pressure drop

Pressure drop (ΔP) is a crucial performance parameter for STHE, as it directly affects the pumping power required to maintain fluid flow. Figure 11 presents the pressure drop for each baffle configuration as a function of mass flow rate.

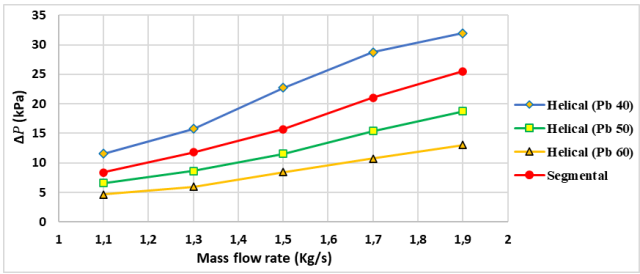

Figure 11. Pressure drop (ΔP) of the variation baffle versus mass flow rate

As expected, the SB exhibits the highest pressure drops across all mass flow rates. This is due to the flow disturbances and flow separation caused by the sharp directional changes imposed by the SB. These sharp flow changes result in large recirculation zones and significant turbulence, leading to higher pressure losses. Such characteristics align with findings reported in Lei et al. [30] and Zhang et al. [18]. The pressure drop increases significantly with the mass flow rate, indicating that the pumping energy required to overcome flow resistance is directly proportional to the flow rate. The SB configuration exhibits a pressure drop that is considerably higher than that of the HB, as expected from previous studies [14].

For the HB, the pressure drop decreases as the baffle pitch increases. The configuration with a 40 mm pitch shows the highest pressure drop due to the tighter spacing between the baffles, which increases flow resistance. However, this configuration also provides the highest heat transfer rate, as discussed in the following section. As the baffle pitch is increased to 50 mm and 60 mm, the pressure drop is significantly reduced. The 60 mm pitch configuration produces the lowest pressure drop among the HB designs, reflecting smoother flow transitions and lower resistance to flow. This result supports the findings of Zhang et al. [9], who showed that HB reduces pressure drop compared to SB while maintaining high heat transfer efficiency.

Interestingly, the increase in pressure drop with the 40 mm pitch HB configuration is particularly prominent, with increases of 149.14%, 164.87%, 169.57%, and 168.86% compared to the 60 mm pitch configuration. This higher pressure drop is due to the tighter spacing between the baffles, which increases flow resistance [11]. Thus, while a smaller pitch enhances heat transfer by promoting more intense turbulence, it also leads to higher pressure drops, necessitating a careful optimization of pitch distance.

3.3 Heat transfer coefficient

The heat transfer coefficient ($\propto_s$) is a key measure of the heat exchanger's thermal performance. As shown in Figure 12, the heat transfer coefficient increases with increasing mass flow rate for all baffle configurations [31]. This trend is associated with the increase in Reynolds number, which enhances turbulence intensity, reduces the thickness of the thermal boundary layer, and improves convective heat transfer on the shell side.

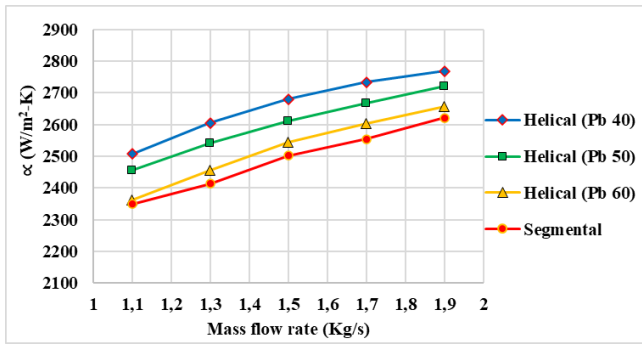

Figure 12. Heat transfer coefficient ($\propto_s$) for variation of baffle configurations versus mass flow rate

The HB with a 40 mm pitch provides the highest heat transfer coefficient, which is a direct result of the intense turbulence and fluid mixing induced by the smaller pitch [18, 30]. On the microscopic level, the tighter pitch generates a continuous helical flow with strong secondary swirling motions, increasing wall shear stress, and continuously renewing the near-wall fluid layer. This mechanism suppresses thermal boundary-layer growth along the tube surface and maintains a high local temperature gradient, significantly enhancing convective heat transfer [32]. However, the increased turbulence and flow velocity also cause a higher pressure drop, making the 40 mm pitch configuration less favorable in terms of energy efficiency and operational cost [33].

The 50 mm and 60 mm pitch HB exhibit lower heat transfer coefficients, with average increases of 4.23% and 1.42%, respectively, compared to the SB configuration. The reduction in heat transfer performance with increasing pitch is attributed to weakened secondary flow structures and partial redevelopment of the thermal boundary layer between successive baffles [34]. Although the 60 mm pitch configuration maintains a heat transfer coefficient comparable to that of the SB, it achieves a significantly lower pressure drop, indicating smoother and more uniform flow behavior. In contrast, SB induces localized turbulence through abrupt flow redirection but generates recirculation and dead-flow zones,

resulting in inferior thermohydraulic performance for a given hydraulic penalty.

3.4 Performance evaluation factor

The PEF was calculated by comparing the heat transfer rate ($\dot{Q}$) and pressure drop (ΔP) for each baffle configuration. These two parameters are closely linked, and their combined effect determines the overall efficiency of the heat exchanger. In an ideal STHE design, higher heat transfer rates ($\dot{Q}$) and lower pressure drops (ΔP) lead to better performance, with lower energy consumption and operational costs. Therefore, the PEF serves as an important metric for evaluating the efficiency of each baffle configuration [12, 27].

As seen in Figure 13**,** the HB with a 60 mm pitch exhibited the highest PEF, demonstrating the most efficient performance. This is because the 60 mm pitch configuration achieved a high heat transfer rate ($\dot{Q}$) while maintaining a very low pressure drop (ΔP), making it the most energy-efficient option. The 60 mm pitch HB configuration strikes the best balance between heat transfer efficiency and pressure drop, leading to lower operational costs due to reduced pumping power requirements [13, 35].

In contrast, the 40 mm pitch HB showed the lowest PEF. While it provided the highest heat transfer rate ($\dot{Q}$), the significant pressure drop caused by the tighter pitch resulted in a lower overall performance. The high pressure drop (ΔP) with the 40 mm pitch configuration leads to increased energy consumption, as more pumping power is required to overcome the flow resistance, thus making it less efficient compared to other configurations.

The PEF analysis also revealed significant performance improvements of the HB compared to the SB. The HB with 50 mm and 60 mm pitches achieved 28.59% and 48.49% higher PEF values, respectively, than the SB configuration. This indicates that HB outperforms SB in both heat transfer efficiency and pressure drop reduction, making them a more energy-efficient choice for industrial applications [36].

On the other hand, the 40 mm pitch HB exhibited a 27.34% decrease in PEF compared to the 50 mm and 60 mm pitch configurations. Although it provides the highest heat transfer, the associated increase in pressure drop reduces its overall efficiency. This highlights the inherent trade-off between heat transfer and pressure drop, where smaller baffle pitches improve heat transfer but increase flow resistance, leading to higher operational costs.

The PEF analysis thus underscores the importance of baffle pitch optimization in STHE. The 60 mm pitch HB emerged as the most optimal configuration, providing the best overall balance of heat transfer efficiency and low pressure drop, which is essential for improving energy efficiency and reducing operational costs in industrial heat exchangers.

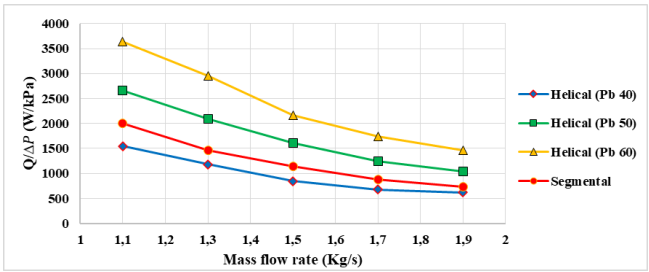

Figure 13. Shell side performance evaluation factor (PEF) of variation baffle versus mass flow rate

Beyond overall thermo-hydraulic efficiency, the performance trends reflected by the PEF provide relevant insights into practical engineering implications for industrial operation. In addition to thermo-hydraulic performance, economic aspects should also be considered when selecting baffle configurations. Although a quantitative cost–benefit analysis was not conducted due to the lack of proprietary industrial cost data and the scope of this CFD-based study, a qualitative assessment can be discussed. SB generally has lower manufacturing costs; however, its higher pressure drop leads to increased pumping power requirements and operational energy costs [37, 38].

HB may involve higher fabrication complexity and initial costs, but their significantly lower pressure drop—particularly for larger pitch distances—can reduce long-term operating and maintenance costs. In particular, the HB with a 60 mm pitch provides a favorable balance between heat transfer performance and pressure drop, indicating promising economic potential when lifecycle operational efficiency is considered. The highest PEF obtained for this configuration is associated with smoother and more continuous shell-side flow characteristics, lower pressure fluctuations, and reduced flow interruption compared to the SB and HB with smaller pitch distances. Such flow conditions play an important role in minimizing stagnant zones, which are known to accelerate particle deposition and fouling during long-term operation.

In addition, the more gradual flow redirection provided by the larger-pitch HB potentially reduces the risk of localized erosion–corrosion caused by high-velocity fluid impingement near baffle edges. From an operational stability perspective, the more stable and continuous flow pattern also contributes to reduced pressure fluctuations and flow-induced vibrations, thereby enhancing mechanical reliability and extending the service life of STHE. Although fouling, corrosion, and long-term stability were not quantitatively evaluated in this study, the simulated flow behavior provides a strong basis for concluding that optimized HB configurations offer advantages not only in energy efficiency but also in operational reliability and sustainability for industrial applications [39].

4. CONCLUSION

This study compared the performance of STHE with different baffle configurations, including SB and HB with pitch distances of 40 mm, 50 mm, and 60 mm. Numerical simulations using ANSYS Fluent were conducted to analyse the heat transfer rate ($\dot{Q}$) and pressure drop (ΔP) across various mass flow rates. The results showed that as mass flow rate increased, both heat transfer coefficient ($\propto_s$) and pressure drop (ΔP) also increased. The 40 mm pitch HB exhibited the highest pressure drop, followed by SB, with the 50 mm and 60 mm pitch HB showing progressively lower pressure drops. In terms of heat transfer, the 40 mm pitch HB provided the highest $\propto_s$, followed by 60 mm HB, 50 mm HB, and SB.

The PEF, which combines heat transfer rate and pressure drop, revealed that the 60 mm pitch HB offered the best balance between high heat transfer and low pressure drop, yielding the highest PEF. This configuration was found to be the most energy-efficient, as it minimized pumping power requirements while maintaining effective thermal performance. The 50 mm pitch HB improved PEF by 28.59% compared to SB, while the 40 mm pitch HB had the lowest PEF due to its high pressure drop, despite its superior heat

transfer performance.

Overall, the study demonstrates the importance of optimizing baffle pitch in STHE to achieve the most efficient performance. The 60 mm pitch HB was identified as the most optimal configuration, providing the best combination of high heat transfer efficiency and low pressure drop. This balance results in significant energy savings and reduced operational costs, making the 60 mm pitch HB the preferred choice for industrial heat exchanger applications.

ACKNOWLEDGMENT

The authors would like to express their sincere gratitude to Kementerian Pendidikan Tinggi, Kebudayaan, Riset dan Teknologi Republik Indonesia for funding this fundamental research (Contract number: 01768/PL8/AL.04/2024). The authors also extend their deepest appreciation to Universitas Pembangunan Nasional Veteran Jakarta and Politeknik Negeri Bali for their valuable resources and facilities throughout this study.

REFERENCES

[1] Fernandes, E.J., Krishanmurthy, S.H. (2022). Design and analysis of shell and tube heat exchanger. International Journal for Simulation and Multidisciplinary Design Optimization, 13: 15. https://doi.org/10.1051/smdo/2022005

[2] Sundén, B. (2007). Computational fluid dynamics in research and design of heat exchangers. Heat Transfer Engineering, 28(11): 898-910. https://doi.org/10.1080/01457630701421679

[3] Master, B.I., Chunangad, K.S., Boxma, A.J., Kral, D., Stehlík, P. (2006). Most frequently used heat exchangers from pioneering research to worldwide applications. Heat Transfer Engineering, 27(6): 4-11. https://doi.org/10.1080/01457630600671960

[4] You, Y., Fan, A., Chen, C., Fang, S., Jin, S., Huang, S. (2012). Numerical study of shellside performance of heat transfer and flow resistance for heat exchanger with trefoil-hole baffles. Advanced Materials Research, 557-559: 2141-2146. https://doi.org/10.4028/www.scientific.net/AMR.557-559.2141

[5] Bell, K.J. (2004). Heat exchanger design for the process industries. Journal of Heat and Mass Transfer, 126(6): 877-885. https://doi.org/10.1115/1.1833366

[6] Gulyani, B.B. (2000). Estimating number of shells in shell and tube heat exchangers: A new approach based on temperature cross. Journal of Heat and Mass Transfer, 122(3):566-571. https://doi.org/10.1115/1.1287159

[7] Li, H., Kottke, V. (1998). Effect of baffle spacing on pressure drop and local heat transfer in shell-and-tube heat exchangers for staggered tube arrangement. International Journal of Heat and Mass Transfer, 41(10): 1303-1311. https://doi.org/10.1016/S0017-9310(97)00201-9

[8] de O. Gonçalves, C., Costa, A.L.H., Bagajewicz, M.J. (2017). Shell and tube heat exchanger design using mixed-integer linear programming. AIChE Journal, 63(6): 1907-1922. https://doi.org/10.1002/aic.15556

[9] Zhang, X., Han, D., He, W., Yue, C., Pu, W. (2017). Numerical simulation on a novel shell-and-tube heat exchanger with screw cinquefoil orifice baffles. Advances in Mechanical Engineering, 9(8). https://doi.org/10.1177/1687814017717665

[10] Kral, D., Stehlik, P., Van Der Ploeg, H.J., Master, B.I. (1996). Helical baffles in shell-and-tube heat exchangers, Part I: Experimental verification. Heat Transfer Engineering, 17(1): 93-101. https://doi.org/10.1080/01457639608939868

[11] Gao, B., Bi, Q., Nie, Z., Wu, J. (2015). Experimental study of effects of baffle helix angle on shell-side performance of shell-and-tube heat exchangers with discontinuous helical baffles. Experimental Thermal and Fluid Science, 68: 48-57. https://doi.org/10.1016/j.expthermflusci.2015.04.011

[12] Almulla, N., Moawed, M., Abd Elrahaman, M., Salem, M. (2024). Effect of baffle configuration on the thermal performance attributes of shell and semi-circular tube heat exchangers. Engineering Research Journal (Shoubra), 53(1): 279-291. https://doi.org/10.21608/erjsh.2023.243772.1236

[13] Sun, Y., Wang, X., Long, R., Yuan, F., Yang, K. (2019). Numerical investigation and optimization on shell side performance of a shell and tube heat exchanger with inclined trefoil-hole baffles. Energies, 12(21): 4138. https://doi.org/10.3390/en12214138

[14] Yang, J.F., Zeng, M., Wang, Q.W. (2015). Numerical investigation on combined single shell-pass shell-and-tube heat exchanger with two-layer continuous helical baffles. International Journal of Heat and Mass Transfer, 84: 103-113. https://doi.org/10.1016/j.ijheatmasstransfer.2014.12.042

[15] Pal, E., Kumar, I., Joshi, J.B., Maheshwari, N.K. (2016). CFD simulations of shell-side flow in a shell-and-tube type heat exchanger with and without baffles. Chemical Engineering Science, 143: 314-340. https://doi.org/10.1016/j.ces.2016.01.011

[16] Xiao, X., Zhang, L., Li, X., Jiang, B., Yang, X., Xia, Y. (2013). Numerical investigation of helical baffles heat exchanger with different Prandtl number fluids. International Journal of Heat and Mass Transfer, 63: 434-444. https://doi.org/10.1016/j.ijheatmasstransfer.2013.04.001

[17] Jafari Nasr, M.R., Shafeghat, A. (2008). Fluid flow analysis and extension of rapid design algorithm for helical baffle heat exchangers. Applied Thermal Engineering, 28(11-12): 1324-1332. https://doi.org/10.1016/j.applthermaleng.2007.10.021

[18] Zhang, J.F., He, Y.L., Tao, W.Q. (2009). 3D numerical simulation on shell-and-tube heat exchangers with middle-overlapped helical baffles and continuous baffles - Part I: Numerical model and results of whole heat exchanger with middle-overlapped helical baffles. International Journal of Heat and Mass Transfer, 52(23-24): 5371-5380. https://doi.org/10.1016/j.ijheatmasstransfer.2009.07.006

[19] Tanujaya, H., Darmawan, S. (2021). Investigation of flow of the disc-and-doughnut baffles and 40% cut segmental baffles. International Journal of Heat and Technology, 39(5): 1541-1548. https://doi.org/10.18280/ijht.390516

[20] Naqvi, S.M.A., Wang, Q. (2019). Numerical comparison of thermohydraulic performance and fluid-induced vibrations for STHXS with segmental, helical, and novel

clamping antivibration baffles. Energies, 12(3): 540. https://doi.org/10.3390/en12030540
[21] Zema, T.B., Dejene, M. (2023). Design and simulation of shell-and-tube heat exchanger (STHE) with the effect of baffles using CFD-tool. Engineering and Technology Journal, 8(5). https://doi.org/10.47191/etj/v8i5.02
[22] He, L., Li, P. (2018). Numerical investigation on double tube-pass shell-and-tube heat exchangers with different baffle configurations. Applied Thermal Engineering, 143: 561-569. https://doi.org/10.1016/j.applthermaleng.2018.07.098
[23] Vukić Mića, V., Tomić Mladen, A., Živković Predrag, M., Ilić Gradimir, S. (2014). Effect of segmental baffles on the shell-and-tube heat exchanger effectiveness. Hemijska Industrija, 68(2): 171-177. https://doi.org/10.2298/hemind130127041v
[24] Pamuk, M.T. (2019). Numerical investigation of the effects of the baffles added in a concentric pipe heat exchanger. International Journal of Heat and Technology, 37(2): 583-588. https://doi.org/10.18280/ijht.370228
[25] Wen, J., Yang, H., Wang, S., Xu, S., Xue, Y., Tuo, H. (2015). Numerical investigation on baffle configuration improvement of the heat exchanger with helical baffles. Energy Conversion and Management, 89: 438-448. https://doi.org/10.1016/j.enconman.2014.09.059
[26] De, D., Pal, T.K., Bandyopadhyay, S. (2017). Helical baffle design in shell and tube type heat exchanger with CFD analysis. International Journal of Heat and Technology, 35(2): 378-383. https://doi.org/10.18280/ijht.350221
[27] Song, S. (2013). Performance study of heat exchangers with continuous helical baffles on different inclination angles. Advanced Materials Research, 655-657: 461-464. https://doi.org/10.4028/www.scientific.net/AMR.655-657.461
[28] Rahmah, L.A., Sa'adiyah, D.S., Sulistijono, S. (2019). Analyze the effects of helical baffles angles variation on shell side heat transfer coefficient and pressure drop of shell and tube heat exchange. SPECTA Journal of Technology, 2(1): 43-52. https://doi.org/10.35718/specta.v2i1.94
[29] Yousfi, M. (2022). Helical baffle thermohydraulic performance versus segmental baffle one. Mechanika, 28(6). https://doi.org/10.5755/j02.mech.31096
[30] Lei, Y.G., He, Y.L., Chu, P., Li, R. (2008). Design and optimization of heat exchangers with helical baffles. Chemical Engineering Science, 63(17): 4386-4395. https://doi.org/10.1016/j.ces.2008.05.044
[31] Parihar, V.S., Pandey, S., Malviya, R.K., Goyal, P. (2023). CFD simulation of helical shell and tube heat exchanger using optimization techniques. Journal of Engineering Research, 11(1): 253-265. https://doi.org/10.36909/jer.11985
[32] Ali, A., Marwat, D.N.K., Ali, A. (2022). Analysis of flow and heat transfer over stretching/shrinking and porous surfaces. Journal of Plastic Film & Sheeting, 38(1): 21-45. https://doi.org/10.1177/87560879211025805
[33] Cucumo M., Ferraro V., Kaliakatsos D., Mele M., Galloro A., Schimio R., Pera G.L. (2016). Thermohydraulic analysis of a shell-and-tube "helical baffles" heat exchanger, International Journal of Heat and Technology, 34(S2): S255-S262. https://doi.org/10.18280/ijht.34S210
[34] Hu, B., Liu, H., Jin, M. (2023). Numerical simulation of thermo-hydraulic behaviour of shell and tube heat exchanger equipped with segmental baffle and helical baffle. Journal of Physics: Conference Series, 2584: 012050. https://doi.org/10.1088/1742-6596/2584/1/012050
[35] Youcef, A., Saim, R., Kourti, M.C., Benhamou, M. (2021). Numerical analysis thermal fluid in a heat exchanger with baffles inclination. Journal of Renewable Energies, 1(1): 237-244. https://doi.org/10.54966/jreen.v1i1.1060
[36] Kumar, A., Zainith, P., Sharma, A., Mishra, N.K. (2023). Numerical investigation on thermal-hydraulic performance of air preheater equipped with helical inserts. Proceedings of the Institution of Mechanical Engineers, Part C: Journal of Mechanical Engineering Science, 237(8): 1968-1979. https://doi.org/10.1177/09544062221134209
[37] Chaoui, A., Bouzid, S., Aidi, M., Bordja, L., Poós, T. (2025). Comparative study of shell-and-tube heat exchanger designs for improved thermal performance and energy efficiency. Advances in Mechanical Engineering, 17(12). https://doi.org/10.1177/16878132251408726
[38] De Carvalho, C.B., De Carvalho, E.P., Ravagnani, M.A.D.S.S. (2022). Optimization of flow rate distribution in a crude oil preheat train considering fouling deposition in shell and tube sides. Industrial & Engineering Chemistry Research, 61(16): 5568-5577. https://doi.org/10.1021/acs.iecr.1c04941
[39] Schlüter, F., Augustin, W., Scholl, S. (2022). Application of experimental data to model local fouling resistances. Heat and Mass Transfer, 58(1): 29-40. https://doi.org/10.1007/s00231-021-03094-x

NOMENCLATURE

A_{cross}	the cross-sectional area representing the cross-lined flow area in the centre of the shell, mm
A_0	the area of the heat exchanger is based on the outside diameter of the tube, mm^2
B_c	baffle cut, %
B_s	baffle spacing, mm
B_t	baffle thickness, mm
C_p	specific heat, J·kg^{-1}·K^{-1}
d_e	equivalent diameter, mm
D_i	shell inside diameter, mm
d_o	tube outside diameter, mm
G	pre flow rate, Kg/s
L	effective tube length, mm
L_H	length of heat exchanger, mm
N_C	the number of tubes in the center row on the shell side
D_n	diameter of inlet and outlet of the shell, mm
N_T	number of tubes
P_r	Prandtl number
P_t	tube pitch, mm
$\dot{Q}$	heat rate, W
R_e	Reynolds number
$S_{i/o}$	inlet and outlet spacing, mm
t	temperature, K
T_t	tube thickness, mm
V_s	average velocity on the shell side, m/s

Greek letters

ρ	density, $kg \cdot m^{-3}$
λ	thermal conductivity, $W \cdot m^{-1} \cdot K^{-1}$
μ	dynamic viscosity, $kg \cdot m^{-1} \cdot s^{-1}$
ΔP_s	static pressure drop
ΔP_d	dynamic pressure drop
$\propto$	heat transfer coefficient
Δt_m	logarithmic mean temperature difference, K

Subscripts

c	cold
h	hot
in	inlet
out	outlet
s	shell side
t	tube side

Abbreviations

CFD	computational fluid dynamics
CH	continuous helical baffle
CMSP	combined multiple shell-pass
CSSP	combined single shell-pass
DTP	double tube-passes
FB	flower baffle
HB	helical baffle
LFT	low-fin tube
RSFT	rib-shaped fin tube
SB	segmental baffle
STHE	shell-and-tube heat exchanger
STP	single tube-passes